# Effect of resin-rich bond line thickness and fibre migration on the toughness of unidirectional Carbon/PEEK joints

Francisco Sacchetti[1,2], Wouter J.B. Grouve[1], Laurent L. Warnet[2], Irene Fernandez Villegas[3]

[1]*ThermoPlastic composites Research Center (TPRC), Enschede, The Netherlands*

[2]*Faculty of Engineering Technology, Chair of Production Technology, University of Twente, Enschede, The Netherlands*

[3]*Structural Integrity and Composites, Faculty of Aerospace Engineering, Delft University of Technology, Delft, The Netherlands*

Palatijn 15, P.O. Box 770, 7500AE Enschede, The Netherlands

Email: Laurent Warnet (email to:l.warnet@utwente.nl), web page: http://www.tprc.nl

# Effect of resin-rich bond line thickness and fibre migration on the toughness of unidirectional Carbon/PEEK joints

*Abstract*

*It is a common practice in fusion bonding of thermoplastic composites to add a matrix layer between the two substrates to be joined. The aim is to ensure proper wetting of the two parts. The effect of this additional matrix layer on the mechanical performance was studied by mode I fracture toughness measurements. The additional matrix was inserted at the interface in the form of films of various thicknesses. Three different manufacturing techniques, namely autoclave consolidation, press consolidation and stamp forming, were used to prepare different sets of specimens with varying resin-rich bond line thickness. The occurrence of fibre migration towards the matrix rich interface was induced by the manufacturing techniques used due to their different processing times. The interlaminar fracture toughness was observed to increase with increasing amount of extra-matrix at the interface, while no effects of the fibre migration on the fracture toughness were observed.*

Keywords: thermoplastic composites, fusion bonding, matrix interleaving, fracture mechanics, fractography

## 1. Introduction

Fusion bonding can be considered as an affordable way to assemble thermoplastic composite parts [1]. From a practical viewpoint, the process involves heating of the interface between the parts, followed by the application of pressure and cooling down. There are many fusion bonding techniques available, all differing in the way heat and pressure are applied to the interface [2, 3]. Two groups of fusion bonding techniques can be distinguished by the size of the area heated, namely bulk heating and welding, which is characterised by local heating. The first group consists of bringing the entire part to melt and using the tooling to maintain pressure throughout the process. Consequently, this technique is characterised by a relatively long processing time (1-2 hours) [4]. The second group is characterised by local heating, and sometimes by local application of pressure, which means that a short processing time can be achieved (minutes or seconds).

From a physical viewpoint, the fusion bonding process involves intimate contact development between the two surfaces (also known as wetting), followed by interdiffusion of polymer chains across the interface (also known as healing) [5]. Proper wetting may be a challenge for thermoplastic composites with a high fibre volume fraction due to the lack of matrix material at the interface; this may result in poor bond performance [6]. To solve this problem, an additional layer of neat polymer can be inserted (interleave) at the interface in order to promote wetting [7, 8, 9]. Moreover, some welding techniques may, in any case, require such an additional resin layer at the interface. For example, a resin layer is added as an energy director in the case of ultrasonic welding, while resistance welding requires a metal mesh embedded in a matrix layer at the interface [5, 10]. This additional layer of pure polymer may lead to a matrix rich bond line which in turn may affect the joint performance. A proper understanding of the interrelation between the matrix rich bond line thickness and the joint performance is required to enable optimisation of the joint design.

Earlier research showed that the interlaminar fracture toughness of Carbon/PEEK increases with interleaving thickness (i.e. with increasing thickness of the matrix rich bond line) [11, 9]. This is in line with the work on other material systems [12, 13, 14, 15] and adhesives joints [16, 17] and is generally related to the size of the plastic yielding zone in front of the crack tip. An increase in matrix interface thickness allows for a larger plastic yielding zone, resulting in a higher interlaminar fracture toughness. It is proposed that the interlaminar toughness eventually reaches a plateau value equal to the matrix toughness for larger matrix interleaved thicknesses [18, 16]. To the best of the authors' knowledge, the aforementioned studies were all performed on samples manufactured using a typical (bulk heating) consolidation technique, i.e. either autoclave or press consolidation. These techniques are characterised by a long processing time, which allows fibres to migrate into the matrix rich area at the interface. The long processing times are not representative of what happens during welding. In this case, the short processing times are expected to significantly reduce fibre migration. It is not clear how this fibre migration affected the measured toughness values reported in the literature. Two effects may play a role, on one hand, fibre migration leads to more fibre-fibre contact, which effectively reduces the plastic zone size and, hence, the fracture toughness [19, 13]. On the other hand, fibre migration may also lead to fibre nesting, resulting in so-called fibre bridging which causes an increase in toughness [20, 21].

In this research, the effect of interleaving thickness and fibre migration on the interlaminar fracture toughness of unidirectional carbon fibre reinforced poly-ether-ether-ketone (Carbon/PEEK) fusion bonded samples was studied. The interleave thickness was varied by adding unreinforced PEEK films of varying thickness at the interface between the laminates, while the extent of fibre migration was varied by using different processes. Two slow processes, autoclave consolidation and press consolidation, and one fast process, stamp

forming, were used to prepare interleaved fusion bonded samples. The slow processes are expected to yield samples with a high degree of fibre migration, while the fast process should prevent significant fibre migration. A mode I double cantilever beam (DCB) test was used to evaluate the fracture toughness of the joint under mode I failure. Fractographic analysis of the samples was performed after mechanical testing to investigate the failure behaviour of the different samples.

## 2. Experimental methods

Sample preparation consisted of two steps. First, laminates were press consolidated following the procedure described below. Second, these laminates were used as substrates for a fusion bonding step in which two substrates were joined to form a sample. The substrates were fusion bonded using three processing technologies as described in this section. Subsequently, the physical state and the interlaminar fracture toughness of the samples was characterised by cross-sectional microscopy and DCB test respectively. The procedures followed to perform these measurements are described in the following sub-sections.

### 2.1. Materials and substrate manufacturing

Press consolidation was used to prepare unidirectional Carbon/PEEK laminates with a stacking sequence of $[0]_{12}$. The material was provided by TenCate and is known as Cetex® TC1200. The fibres used in the prepreg is a T300 JB 3K while the polymer is a Victrex PEEK 150. The prepreg was stacked in a picture frame mould of 300 by 300 $mm^2$ and subsequently consolidated using a static Pinette Emidacau Industries press following the consolidation cycle suggested by TenCate, which is shown in Figure 1. To ensure deboning of the laminates from the mould, Marbocote® 227CE, a silicon based semi-permanent mould release agent was used as a release media. These laminates were then used as the substrates for the fusion bonding processes.

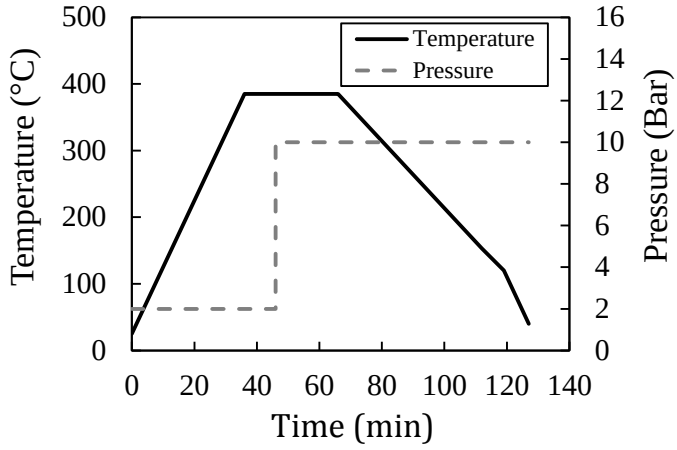


Figure 1: Press cycle used to manufacture the laminates.

## 2.2. Fusion bonding processes

Three different processing techniques were used to prepare the fusion bonded samples, i.e. autoclave consolidation, press consolidation and stamp forming. Regardless of the processing method, a sample was prepared by stacking two substrates on top of each other with optionally additional PEEK film inserted at the interface. The film was manufactured by Victrex and is known under the tradename APTIV®. It was available in two different thicknesses, namely 38 µm and 100 µm. Moreover, a 13 µm thick polyimide film was also inserted between the substrates prior to fusion bonding in order to introduce the pre-crack required for DCB testing. It is worth to notice that in the area where the polyimide film was inserted the additional PEEK films were not inserted. The remainder of this section describes each of the aforementioned processing techniques.

### *2.2.1. Autoclave consolidation*

An autoclave consolidation process was used to fusion bond the first sample set. Seven samples were prepared. The first sample was prepared without an additional film at the interface, while for the other six samples, one to six layers of film with a thickness of 38µm were inserted at the interface prior to consolidation.

A schematic illustration of the autoclave table preparation can be found in Figure 2. The press

consolidated substrates were cut into square sections of 150 by 150 $mm^2$ and subsequently stacked together with the required film material. Brass picture frames with different thicknesses were used as a shim at the interface to maintain the distance between substrates and thereby to prevent the added matrix from being squeezed out. A 10 mm thick aluminium caul sheet was used to ensure the flatness of the laminate. After wrapping the table in a vacuum bag, the substrates were fusion bonded in an autoclave at 6 bar pressure and a temperature of 380 °C based on the process cycle recommended by TenCate, which is shown in Figure 3.

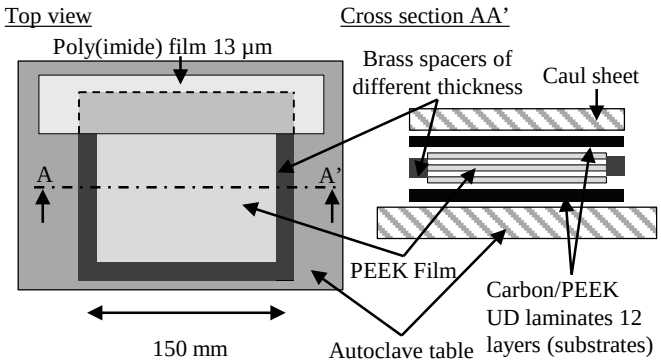


Figure 2: Sketch of the preparation of the autoclave table. In the top view, the upper substrate is not shown for clarity.

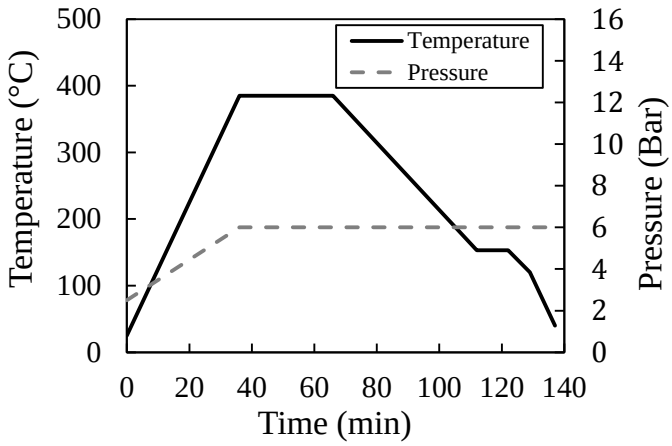


Figure 3. Autoclave consolidation cycle used to fusion bond the substrates.

### *2.2.2. Press consolidation*

A second sample set was prepared by press consolidation of two substrates in a press using a 300 by 300 $mm^2$ picture frame mould. A total of three samples were prepared: one without an additional polymer film, one with a 38 µm PEEK film and one with a 100 µm PEEK film. Contrary to the autoclave consolidation process, no shims or spacers were added as any squeeze flow was restricted by the picture frame mould. The consolidation cycle was the same as the one used to manufacture the substrates i.e. the cycle as shown in Figure 1.

### *2.2.3. Stamp forming*

The last sample set was prepared by using a Pinette Emidacau Industries stamp forming set up to fusion bond two substrates. Two substrate laminates were stacked and placed on a polyimide film of 50 µm thickness, meant for carrying the laminates from the material loading position to the infrared oven and from the oven to the pressing/stamping position. The infrared oven was set at a temperature of 450 °C. The substrates were heated up to complete melting (the temperature at the interface between the two laminates was measured to be 400 °C, taking around 4 minutes of heating time). Then, the substrates were transferred to the stamping station where they were fusion bonded and consolidated between two flat aluminium moulds with a dimension of 250 by 250 $mm^2$. The mould temperature was set to 220 °C. The mould halves were quickly closed, and a pressure of 10 bar was applied for 1 minute. The measured temperature and pressure during stamp forming are illustrated in Figure 4. Three samples were prepared: one without extra polymer, one with a 38 µm PEEK polymer film and one with a 100 µm PEEK polymer film at the interface between the two laminates. Table 1 summarises all the samples that were prepared.

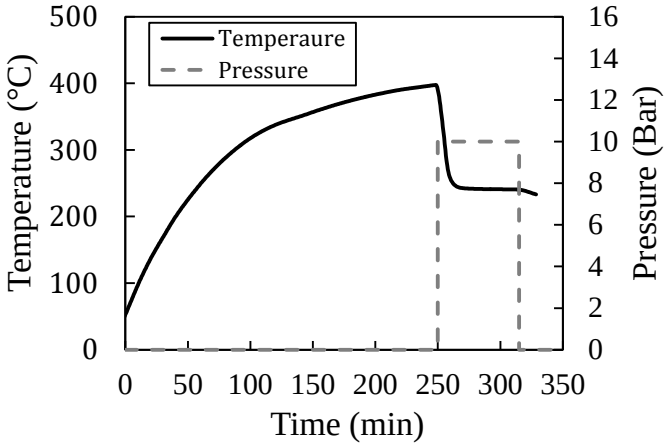


Figure 4: Measured temperature and pressure during stamp forming process.

| Number and thickness (μm) of PEEK film plies | Fusion bonding technique/ Sample name | | |
|---|---|---|---|
| | Autoclave | Press | Stamp-forming |
| None | A-None | P-None | S-None |
| 1 x 38 μm | A-1x38 | P-1x38 | S-1x38 |
| 2 x 38 μm | A-2x38 | - | - |
| 1 x 100 μm | - | P-1x100 | S-1x100 |
| 3 x 38 μm | A-3x38 | - | - |
| 4 x 38 μm | A-4x38 | | |
| 5 x 38 μm | A-5x38 | | |
| 6 x 38 μm | A-6x38 | | |

Table 1: Sample description, the thickness of interleaving, and fusion bonding technology used.

## 2.3. Characterization

After fusion bonding, cross-sectional micrographs of the samples were prepared. Subsequently, double cantilever beam (DCB) tests were performed followed by a fractography analysis.

### *2.3.1. Cross-sectional microscopy*

The consolidation quality of the fusion bonded samples was characterised using thickness measurements and cross-sectional microscopy. The micrographs were taken close to the edge of the fusion bonded laminates, while the centre was kept for mechanical testing, as it is shown in Figure 5. The microscopy images were also used to evaluate, in a qualitative manner, the thickness of the matrix rich bond line and the degree of fibre migration at the

interface.

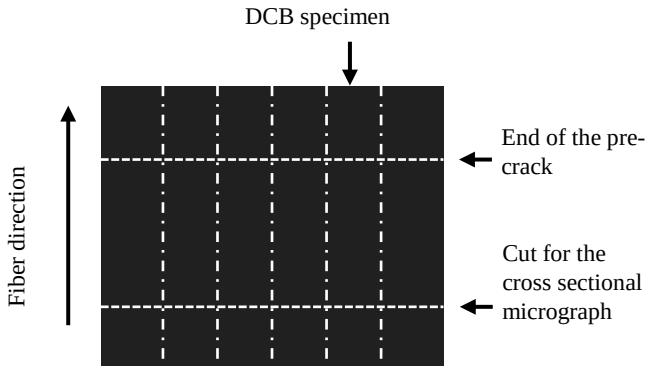


Figure 5: Sketch of the location of the cross-sectional sample preparation and the position of the DCB samples

### *2.3.2. Double cantilever beam experiments*

The interlaminar fracture toughness of the bond line was evaluated using the double cantilever beam (DCB) test method. DCB specimens were cut from the fusion bonded samples in the longitudinal direction of the fibres and then tested according to ISO 15024 [22]. The ISO Standard 15024 is based on the linear elastic fracture mechanics (LEFM). As such, the conformance of the linear elastic behaviour of the specimens during testing was evaluated. Figure 5 shows schematically the location of the test specimens cut to a width of 20 mm from the fusion bonded laminates. The specimens were loaded in a servohydraulic Instron 8500 universal testing machine equipped with a 1 kN force cell. A mode I pre-cracking procedure was performed for all the specimens according to the standard. The specimens were loaded at a constant speed of 1.2 mm/min until a delamination crack growth of about 5 mm has occurred, followed by the specimens unloading until zero force. Next, the specimens were re-loaded at the same constant speed of 1.2 mm/min until the final delamination length of about 100 mm has been reached. A travelling recording camera was used to measure the delamination crack length during testing. The corrected beam theory (CBT) was used to analyse the data. The interlaminar fracture toughness was calculated as:

$$G_{\mathrm{IC}} = \frac{3P\delta}{2w(a+\Delta)}\left(\frac{F}{N}\right), \tag{1}$$

where $P$ is the force, $\delta$ is the displacement, $a$ is the crack length, $w$ is the width of the specimen, $F$ is a correction factor for large displacement, $N$ is a correction factor for the loading blocks and $\Delta$ is a correction factor for the rotation of the beam at the crack tip. Since the delamination length was measured using the horizontal position of the travelling camera system, there is no need for a large-displacement correction factor ($F$) to be applied to the measurements [22] (i.e. $F$ can be considered equal to one). The interlaminar fracture toughness was calculated both for initiation and propagation. The initiation values were calculated following the procedure called 5 % / MAX point in the ISO 15024 standard. From that point on the values measured were considered as propagation values.

### *2.3.3. Fractography analysis*

Two cross-sectional optical micrographs were prepared after testing. One with a sectioning plane perpendicular to the crack propagation direction and the other with a sectioning plane at 20° with respect to the crack propagation direction. A schematic view of how these cross-sectional cuts were taken is shown in Figure 6. All the micrographic specimens were embedded in epoxy and then polished. A Leica DMRX and a Keyence VHX optical microscope were used to obtain the optical micrographs. Moreover, SEM micrographs of the fracture surface were made with a Jeol Neoscope JCM-5000. The cross-sectional and fractography images were analysed in order to determine the crack propagation path and to identify the main failure modes.

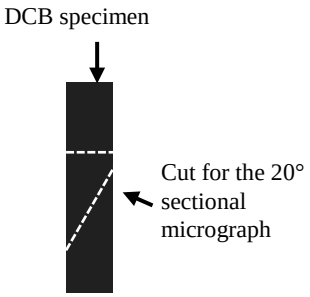


Figure 6: Sketch of the location of cross section micrograph cuts for the fractography analysis

## 3. Experimental results

The experimental results are elaborated in the present section. First, the physical state of the samples and bond line microstructure will be evaluated. Subsequently, the fracture toughness data is provided, followed by the fractographic analysis.

### 3.1. Physical state of the samples

The fusion bonded samples prepared using the autoclave consolidation process showed non-uniform thickness, with the centre of the laminates being thicker than the edges. Despite their thickness (10 mm), the aluminium caul sheets were bent and permanently deformed during the autoclave cycle as a result of the high pressure applied. In some case, the difference in thickness between the edge and the centre was up to 0.15 mm. The quality of the samples manufactured using press consolidation and stamp forming process, in terms of variation in sample thickness, was superior to the autoclaved samples with the variation in thickness being always less than 0.05 mm.

Typical cross-sectional micrographs for the three fusion bonding techniques and with different interleave thicknesses are presented in Figure 7. All micrographs showed good consolidation quality with no voids in the substrates or the interface. For the cases in which a PEEK film was inserted between the laminates prior to fusion bonding, two different regions can be distinguished in all the micrographs shown in Figure 7, i.e. a matrix poor region mainly in the substrates, and a matrix rich region at the bond line. Besides, two different morphologies can be identified in the matrix rich region. The first is characterised by matrix material in which many fibres are randomly distributed as shown in the first and second columns in Figure 7. This morphology arises when fibres migrate, during processing, from the substrates into the interleaved film at the interface. This happened during the slower processes, i.e. during autoclave and press consolidation. The second morphology is

characterised by matrix material with very few or no fibres. This is evident in the stamp formed samples (last column in Figure 7), for which there is not enough time for the fibres to migrate during processing.

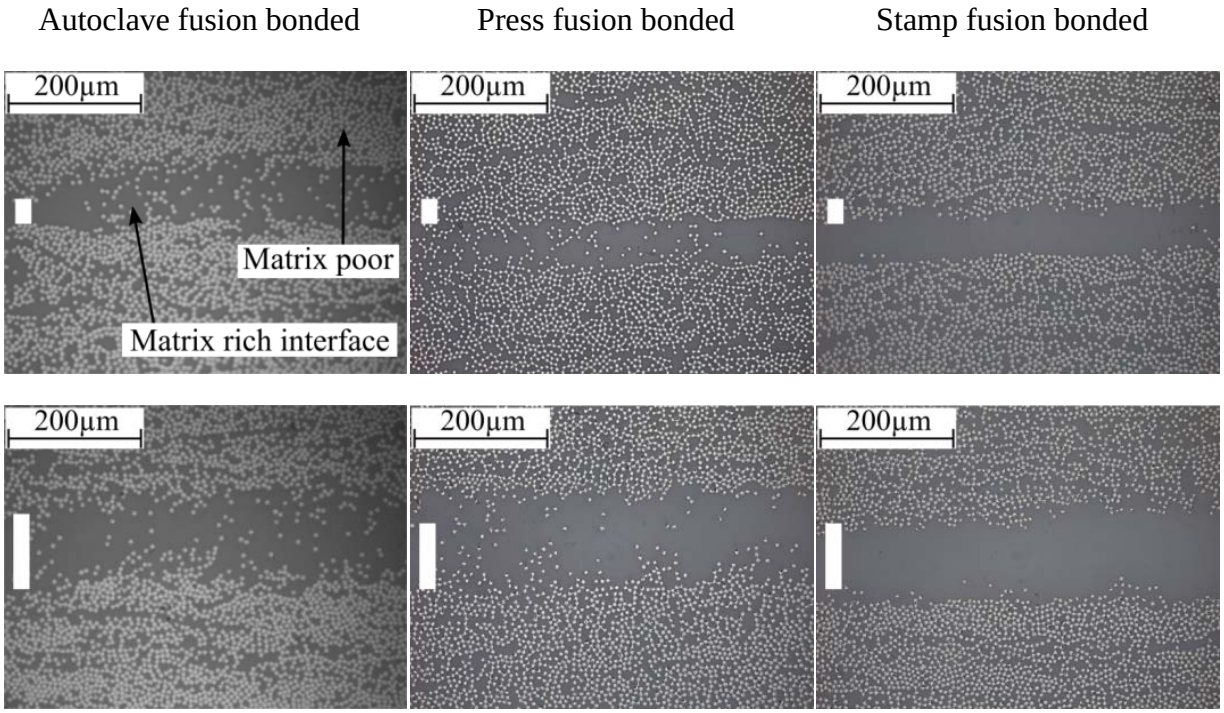


Figure 7: Cross-sectional micrographs of 6 different specimens close to the interface. Left to right: autoclave consolidated specimen, press consolidated specimen, and stamp formed specimen. Top row: specimen interleaved with a 38 µ m thick film. Bottom row: specimen interleaved with 100 µ m film in the case of press consolidation and stamp forming, specimen interleaved with 3 layers of 38 µ m thick films in the case of autoclave consolidation. The white bar on the left of the micrograph indicates the thickness of the interleaved films before processing.

The thickness of the matrix rich region was not uniform along the cross-sectional plane for the autoclaved specimens, which was associated with significant matrix flow during processing. The effect of this non-uniformity on toughness will be further elaborated in the next section. On the contrary, the press consolidated, and the stamp formed samples showed a more uniform thickness of the matrix rich region.

### 3.2. Double cantilever beam experiments

This section presents the results of the DCB experiments. First, the issues encountered during testing are described and examples of force vs. displacement curves are shown. At the end of

this section, the results from all the samples tested are combined to generate a plot of fracture toughness as a function of interleaving thickness.

### *3.2.1. General observations during DCB testing.*

Five DCB specimens were tested for each sample. Nevertheless, several issues were encountered during DCB testing which made the analysis difficult and reduced the number of specimens kept for the analysis. The main problems encountered were instability of crack propagation and the presence of a non-flat resistance curve (toughness vs. crack length). The former leads to a small number of propagation values, making the specimen less statistically relevant, while the latter indicates possible variations in crack propagation mechanisms, such as for example fibre bridging. As both complicate data reduction, two criteria were implemented to obtain a set of specimen data for analysis. A specimen was kept for analysis in case it showed i. at least 10 mm of stable crack propagation, and ii. less than 20% variation in interlaminar toughness along the 10 mm of crack propagation. An exception to the second criteria was made for the stamp formed specimens. The threshold was changed to 50% in order to have enough specimens for analysis. It is worth to notice that only few stamp formed specimens were kept for the analysis which were close to the second criterion. These criteria led to only three to four consistent specimens from an initial lot of five specimens per sample. An exception was the sample from the autoclave which was interleaved with three 38 µm films. Out of the five specimens tested, only two were kept for the analysis. Table 2 summarises the number of specimens discarded and the reason for not using the data. The last column shows the number of specimens kept for the analysis. From the table, it can be noted that the standard samples, i.e. the autoclave and press consolidation samples without interleaving, did not present any problem during testing and all the specimens were kept for the analysis, while all the samples that were manufactured by a nonconventional procedure,

280 i.e. stamp forming or consolidation with interleaving, showed at least one discarded
281 specimen.

| Sample Name | Number of specimens | | | |
|---|---|---|---|---|
| | Presented at least one point of unstable crack propagation | Did not show at least 10 mm of stable crack propagation | More than 20% or 50% derivation in R-curve | Used for the analysis |
| Autoclave | | | | |
| A-None | 0 | 0 | 0 | 5 |
| A-1x38 | 1 | 1 | | 4 |
| A-2x38 | 5 | 2 | | 3 |
| A-3x38 | 4 | 3 | | 2 |
| A-4x38 | 4 | 1 | | 4 |
| A-5x38 | 3 | 1 | | 4 |
| A-6x38 | 3 | 2 | | 3 |
| Press | | | | |
| P-None | 0 | 0 | 0 | 5 |
| P-1x38 | 3 | 1 | | 4 |
| P-1x100 | 2 | 1 | | 4 |
| Stamp | | | | |
| S-None | 2 | 0 | 1 | 4 |
| S-1x38 | 4 | 0 | 1 | 4 |
| S-1x100 | 4 | 0 | 2 | 3 |

282 Table 2: Overview of the number of specimens discarded and the reason for not using the data. The last
283 column shows the number of specimens used for analysis.

284 Two characteristic force - displacement and crack length - displacement curves are shown in
285 the upper graphs of Figure 8. The left graph corresponds to a specimen which showed stable
286 crack propagation, while the right graph belongs to a specimen which showed a combination
287 of stable and unstable crack propagation. During the evaluation of the initiation point, the
288 maximum force point occurs almost always before the 5% point. Furthermore, almost no
289 residual displacement was observed after the specimens were unloaded. The previous two
290 observations means that the material can be analysed according to LEFM by following the
291 ISO15024 standard. Fibre bridging was not observed during testing.
292 The R-curves corresponding to the four specimens are shown in the bottom row of Figure 8.
293 As shown, only the stable part was used to calculate the interlaminar fracture toughness. The
294 first point of the R-curve corresponds to the initiation value for interlaminar fracture

toughness. It can be noted that stable crack propagation is correlated with a continuous R-curve, whereas in the presence of an unstable crack propagation the R-curve is interrupted and therefore shows separate segments.

299

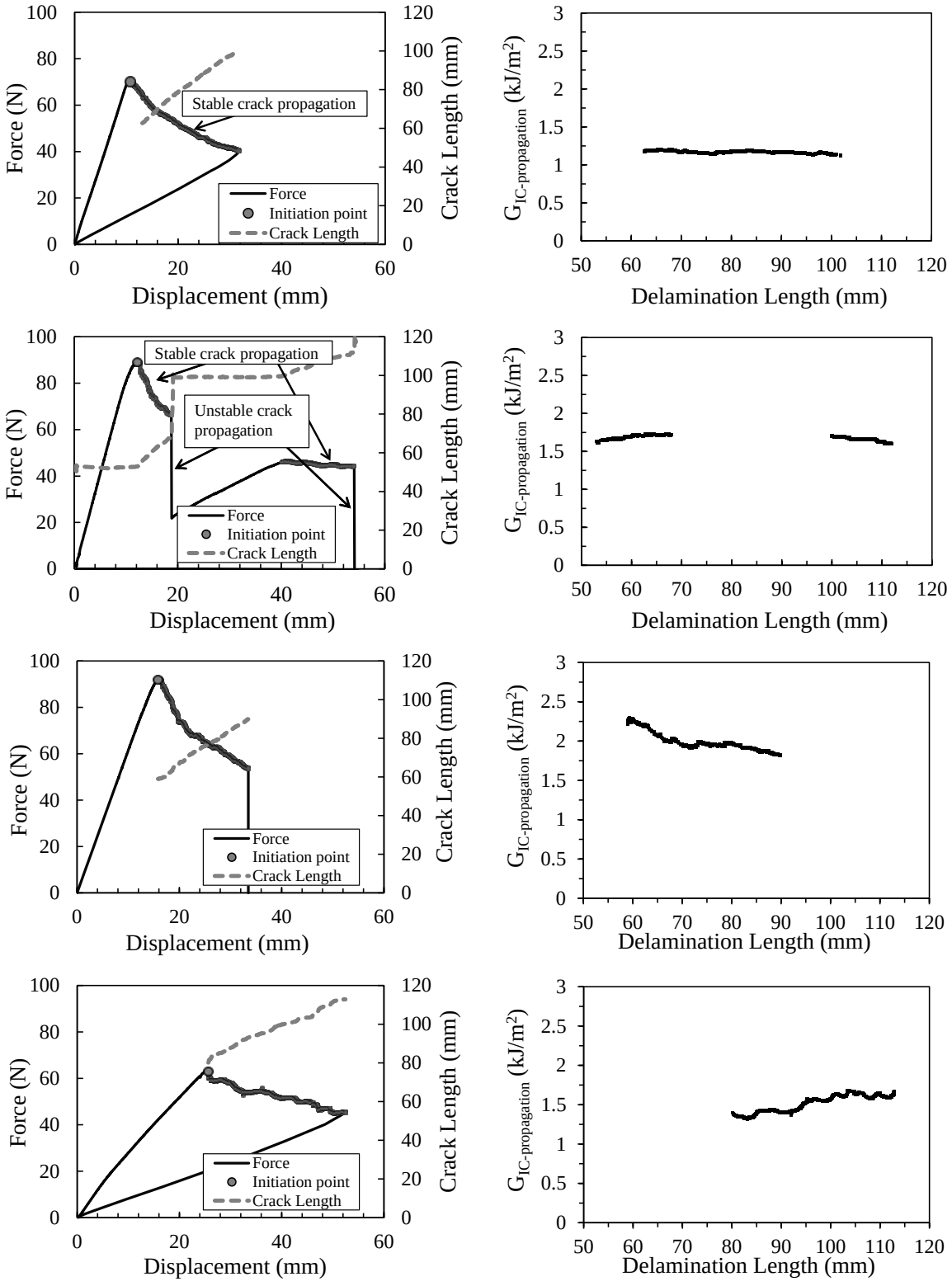


300 Figure 8: Left column: Force-displacement curve and crack length vs displacement. Right column:
301 Interlaminar fracture toughness as a function of crack length (R-curves). First row: Press consolidated specimen
302 that showed only stable crack propagation. Second row: Autoclave specimen that showed a combination of
303 stable and unstable crack propagation. Third row: Autoclave specimen that showed a descending R-curve.
304 Fourth row: stamp forming specimen that showed an ascending R-curve.

Many of the autoclave consolidated specimens suffered from unstable crack propagation as was illustrated in Table 2. Moreover, some of the specimens showed non-uniform toughness along the crack length. In those cases, the trend of the R-curve was mostly decreasing. Although the press consolidated specimens also suffered from unstable crack propagation, they showed longer paths of stable crack propagation compared to the autoclave consolidated samples. Moreover, the R-curves observed in press consolidated specimens were flatter than the ones observed for the autoclave consolidated samples. Finally, the stamp formed samples despite several cases of unstable crack propagation showed a long path of stable crack propagation. Some of these specimens showed a rising R-curve, which in some cases was too large (more than 50%), leading to the rejection of these specimens for the analysis.

The origin of the unevenness in the R-curves observed in the autoclave and stamp formed specimens were attributed to two different phenomena. For the case of the Autoclave samples the decreasing R-curve could be caused by a decreasing interleave thickness towards the end of the specimen, which is the result of resin outflow during processing. The non-flat R-curves of stamp-formed specimens may be related to variations in consolidation quality. Although no voids were observed in the specimens, the degree of healing may vary from place to place. As the process is highly non-isothermal, it is difficult to control temperature during the process. However, a complete picture requires an in-depth investigation, which is deemed to be out of scope of this paper.

#### *3.2.2. Fracture toughness vs. interleaved thickness*

The results of all the samples tested are summarised in Table 3. An average initiation and propagation fracture toughness values were calculated for all the samples. The average initiation value of each sample was calculated by averaging the initiation values of all the specimens within one sample. The average propagation value per sample was determined by

329 averaging the mean propagation value of each specimen within that sample.

330 The last column of Table 3 shows the overall trend of the R-curve for each sample, i.e.
331 whether the R-curve was observed to be flat (-), ascending (/) or descending (\). It can be seen
332 that the trend of the R-curve is closely related to the relation between initiation and
333 propagation. In the cases of a flat R-curve the initiation and propagation values are similar,
334 whereas with an ascending R-curve initiation values are lower than propagation, and the
335 opposite occurs with a descending R-curve.

| Sample type, name | Fracture Toughness ($G_{IC}$) | | R-curve trend |
|---|---|---|---|
| | Initiation (kJ/m$^2$) | Propagation (kJ/m$^2$) | |
| Autoclave | | | |
| A-None | 1.28 ± 0.10 | 1.30±0.10 | - |
| A-1x38 | 1.59 ± 0.10 | 1.55±0.10 | - |
| A-2x38 | 1.87 ± 0.16 | 1.89±0.12 | - |
| A-3x38 | 1.93 ±0.20 | 2.05±0.16 | - |
| A-4x38 | 2.46 ±0.30 | 2.22±0.18 | \ |
| A-5x38 | 2.74 ±0.15 | 2.61±0.15 | \ |
| A-6x38 | 2.85 ±0.28 | 2.66±0.20 | \ |
| Press | | | |
| P-None | 1.17±0.10 | 1.19±0.10 | - |
| P-1x38 | 1.54±0.10 | 1.51±0.10 | - |
| P-1x100 | 2.06±0.17 | 2.12±0.18 | - |
| Stamp | | | |
| S-None | 1.10±0.37 | 1.25±0.25 | / |
| S-1x38 | 1.57±0.15 | 1.60±0.10 | / |
| S-1x100 | 1.80±0.20 | 1.84±0.25 | / |

336 Table 3: Fracture toughness values for initiation and propagation for all the sample tested. The error was
337 calculated as one standard deviation of the set of values within one sample.

338 Initiation and propagation fracture toughness as a function of the interleaved PEEK film
339 thickness is shown in Figure 9 for the three different process technologies used. It is worth
340 noticing that the x-axis is the nominal thickness of the added films and not the actual matrix
341 rich bond line thickness after processing, which in some cases may be smaller due to outflow
342 of matrix. Measurements of the actual matrix rich bond line thickness were difficult to
343 perform from the micrograph and therefore not used. The trend is similar for all three
344 processes, where the fracture toughness increases with increasing interleave thickness. No

significant differences can be observed between the three processes and between initiation and propagation. Despite the similar average toughness values, the stamp forming process resulted in a higher scatter within the sample. This may be due to a non-uniform pressure and temperature distribution during fusion bonding, which may locally have resulted in incomplete wetting or healing.

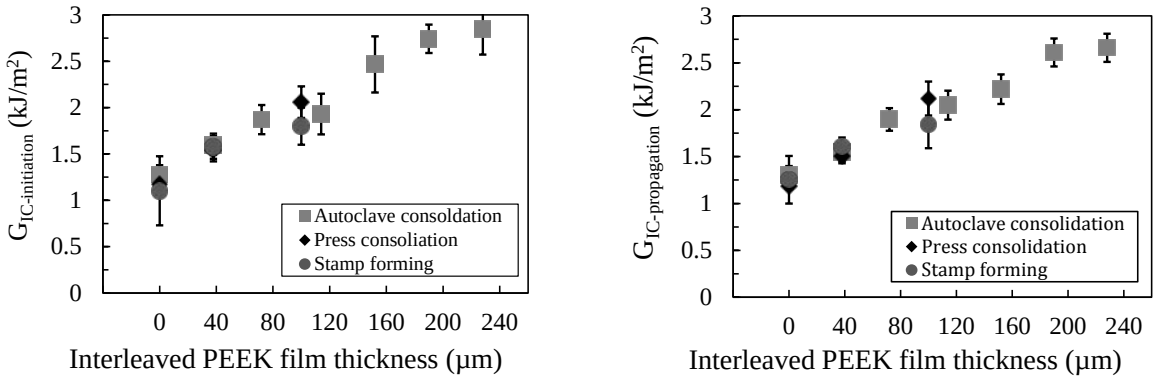


Figure 9: Interlaminar fracture toughness as a function of interleaved thickness for the three processes, autoclave consolidation, press consolidation, and stamp forming.

### 3.3. Fractography

The fracture behaviour of the different samples is compared in this section using cross-sectional micrographs and fractography analysis. First, a comparison between samples without film interleaving and with film interleaving is shown. Later, the comparison between samples with fibre migration and without fibre migration is presented. Three types of images were used for the analyses. Figure 10 shows cross-sectional micrographs perpendicular to the crack propagation direction. These micrographs show the position of the crack at a single instant, though they do not give information about how the crack propagates along the length of the specimen. Figure 11 shows pictures of the optical cross-sectional micrographs with the cross-sectional plane oriented at $20^o$ with respect to the crack propagation direction. These pictures show how the crack propagates through the specimen. Finally, Figure 12 shows the SEM micrographs of the fracture surfaces where the interaction between fibre and matrix and the deformation of the matrix after testing can be observed.

The comparison between samples with and without PEEK film interleaving is presented here. Due to the similarity among the images within each test group, only one representative micrograph per group is shown. The left micrograph in Figure 10 shows a specimen without interleaving. It can be seen that the crack is located at the centre plane of the specimen. The right micrograph shows a specimen with interleaving. In this case, the crack is located close to the interface between the fibre rich and the matrix rich region, slightly out of the centre of the specimen. Other images in the same cross-sectional plane, thus to the left or right of the presented image, showed the same crack at the interface between matrix rich region and the matrix poor region of the upper substrate.

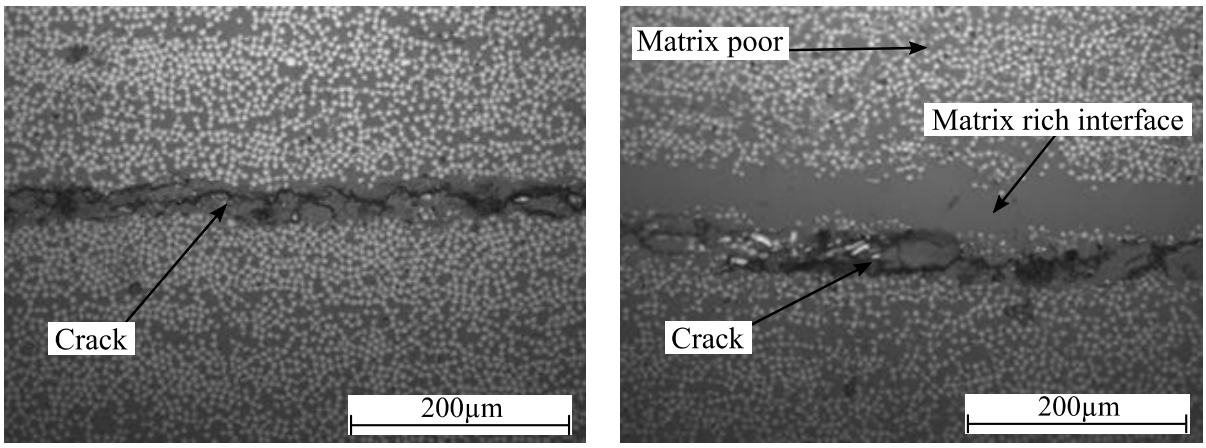


Figure 10: Cross-sectional micrographs perpendicular to the crack propagation direction. Left) autoclave consolidated specimen without interleaving. Right) stamp formed specimen with interleaving.

The straightness of the crack along the propagation direction was analysed using the $20^{o}$ cross-sectional micrographs. The top micrograph in Figure 11 shows a non-interleaved specimen, while the bottom shows an interleaved specimen. It can be noted that the crack path remains flat when the specimens are not interleaved as is shown in the top. However, the crack propagates with some waviness, seemingly avoiding the matrix rich region in the centre, and this is the case for interleaved specimens shown in the bottom image.

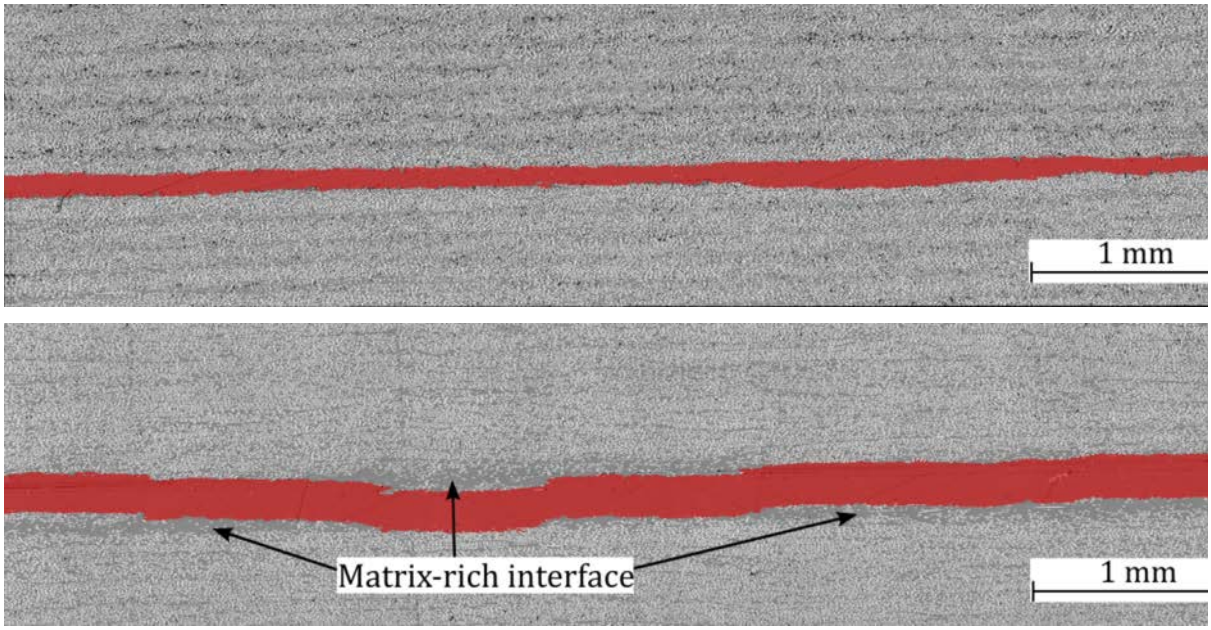


Figure 11: Cross-sectional micrographs were taken at 20$^{o}$ with respect to the crack propagation direction. Top: Non-interleaved stamp formed specimen. Bottom: 100 μ m interleaved press consolidated specimen. The crack is highlighted in red.

A comparison between the fracture surface of an interleaved and a non-interleaved specimen is shown in Figure 12, while Figure 13 shows a schematic illustration of the accompanying cross-section. The SEM image on the left shows that the fracture surface of a non-interleaved specimen is characterised by fibre imprints in the matrix and bare fibres. Also, microscale out of fracture plane plastic deformation of the matrix can be observed, which is a typical feature of the fracture surface of carbon/PEEK laminates tested in mode I [23]. This deformation is present at the edges of the fibres in the schematic view. The SEM micrograph on the right shows that the fracture surface of an interleaved specimen is characterised by two distinct regions. The first region shows a combination of fibre imprints in the matrix and bare fibres, similar to the case of the non-interleaved sample. The second region is characterised by a matrix rich area where large microscale plastic deformation of the matrix can be observed as evidenced by the white polymer regions.

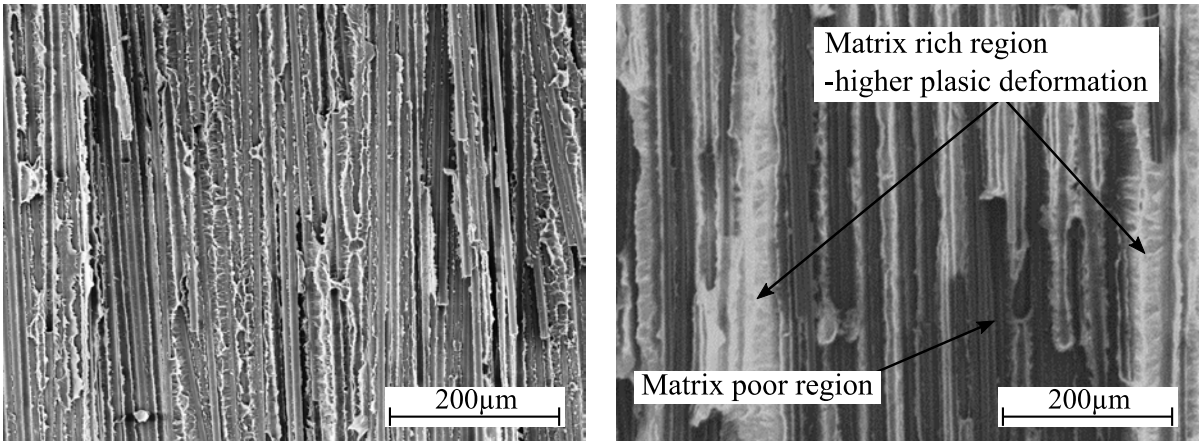


405 Figure 12: Scanning electron micrograph of the fracture surfaces. Left: Autoclave consolidated specimen
406 with no interleaving. Right: interleave press consolidated specimen.
407

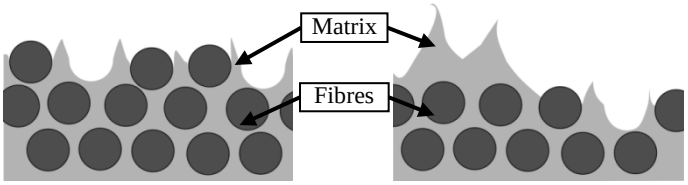


408 Figure 13: Schematic view of a cross-section of a fracture surface. Left: Sample without matrix interleaving.
409 Right: Sample with matrix interleaving [Figure 13 near here]

410 The interleaved samples can be subdivided into two groups. The first comprises the samples
411 prepared using a slow process (autoclave and press consolidation), while the second group
412 consists of samples manufactured using the fast process (stamp forming). Figure 14 and
413 Figure 15 show the cross-sectional micrographs and their schematic illustration for both
414 groups, respectively. The crack shape and location look similar for both cases, irrespectively
415 of whether fibre migration occurred or not. The crack seems to remain at the interface
416 between the matrix rich and matrix poor region. The crack path was observed to alternate
417 between the top and the bottom substrate trying to minimise the crack path length through the
418 matrix rich region, similar to what is observed in Figure 11.

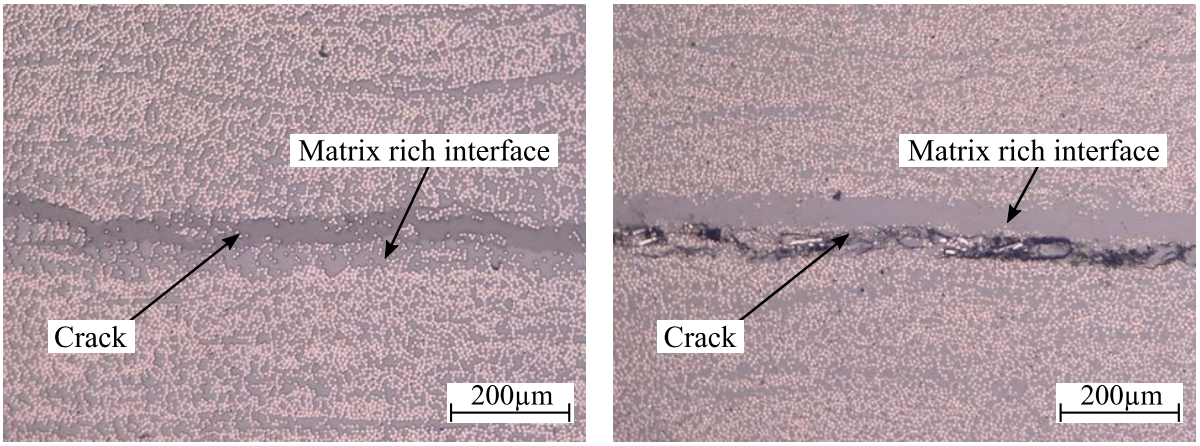


Figure 14: Cross-sectional micrographs perpendicular to the crack propagation direction. Left) autoclave consolidated specimen with interleaving. Right) stamp formed specimen with interleaving.

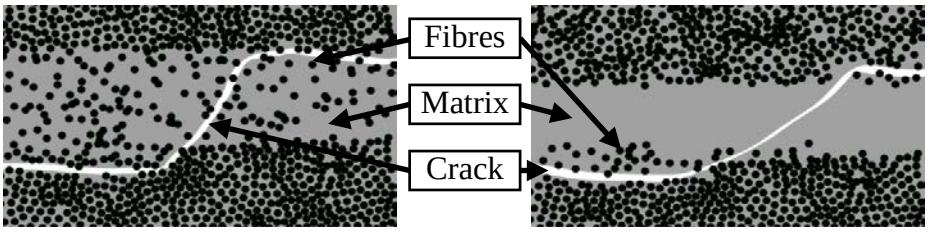


Figure 15: Schematic view of a cross-section micrograph of an interleaved specimen. Left: Specimen with fibre migration as obtained using autoclave or press fusion bonding. Right: Specimen without fibre migration as obtained using stamp fusion bonding.

## 4. Discussion

In this section, the results obtained are combined and discussed with the purpose of getting a deeper understanding of the mechanisms that govern the interlaminar fracture toughness of fusion bonded joints that present a matrix rich bond line.

The interlaminar fracture toughness improves by increasing the matrix rich bond line thickness, as was expected. This is true even if the crack does not propagate through the matrix rich area but through the matrix poor area or the interface between the matrix-poor (one of the two substrates) and matrix-rich (the interleave) regions. This phenomenon was explained by Hojo et al. [13] for interleaved laminates, who reasoned that by increasing the interleave thickness, even if the crack does not propagate fully through the matrix rich area, the plastic yield zone in front the crack tip is still less constrained by the fibres and is

436 therefore allowed to increase in size. Moreover, it was proposed that when the matrix rich
437 region is smaller than the maximum plastic yield zone size, the crack path migrates towards
438 the weakest region, i.e. the boundary between matrix poor and matrix rich regions, resulting
439 in adhesive failure [13]. However, when the thickness of the matrix rich region increases
440 further than the plastic yield zone, the crack will remain within this region resulting in a
441 cohesive failure of the interleave [13]. The change in plastic zone size and the position of the
442 crack propagation path is schematically represented in Figure 16. A larger plastic yield zone
443 area means that more energy will be dissipated, which is reflected by a higher interlaminar
444 fracture toughness. The SEM fractography, as presented in Figure 12, confirmed that more
445 plastic deformation is observed in the interleaved samples compared to the samples without
446 additional matrix at the interface. Besides, the tortuosity of the crack path, as shown in the
447 lower micrograph in Figure 11, may also contribute to an increased fracture toughness

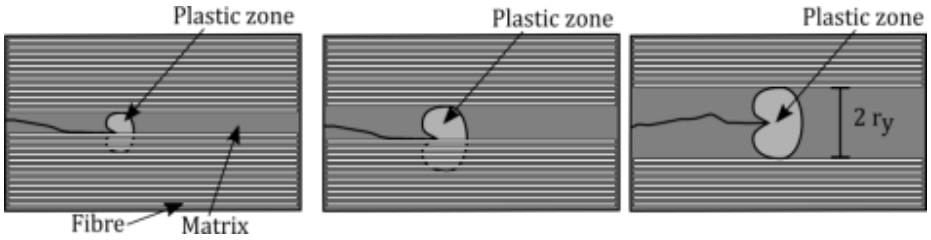


448 Figure 16: A schematic explanation of crack growth behaviour and plastic zone development having a radius
449 $r_y$. Left) Base material, no interleaved. Centre) Material with an interleaving thickness below maximum plastic
450 yield zone ($2r_y$). Right) Material interleaved with a thickness above the maximum plastic yield zone. Figure
451 adapted from [13].

452 Plastic deformation of the matrix was found to be the main mechanism to increase the
453 interlaminar fracture toughness of the interleaved specimens. Nevertheless, as the plasticity is
454 localised only at the fracture surface, the global linear elastic behaviour of the specimen
455 during testing was retained. As such, the tests still comply with the LEFM assumption, which
456 makes the comparison of the values obtained for the different samples acceptable.
457 It was suggested that the maximum theoretical toughness of an interleaved system is the
458 toughness of the pure polymer, which is reached when the interleave thickness is equal or

larger than two times the plastic yield radius (Figure 16 right) [16, 18]. A first approximation of the plastic zone radius ($r_y$) of a polymer can be calculated following Irwin's plastic zone model for plane strain reported by Ozdil and Carlsson [19] (Equation (2)).

$$r_y = \frac{1}{4\pi}\left(\frac{K_{IC}}{\sigma_y}\right)^2 \left(\frac{3}{2}(1-2v^2)\right), \quad (2)$$

where $K_{IC}$ is the stress intensity factor which relates to the fracture toughness of the polymer, $\sigma_y$ is the tensile yield stress of the polymer, and $v$ is the Poisson's ratio. The following expression can be used to relate the stress intensity factor $K_{IC}$ to the energy release rate $G_{IC}$ in case of a plane strain situation:

$$G_{IC} = \frac{(1-v^2){K_{IC}}^2}{E}, \quad (3)$$

where $E$ is the elastic modulus of the polymer. Material data from the literature is required to calculate the maximum theoretical fracture toughness of this system. The following values were reported in the data sheet of Victrex PEEK 150, which is used as matrix in the prepregs; tensile yield point ($\sigma_y$) of 105 MPa, an elastic modulus (E) of 3.5 GPa and a poisson's ratio (v) of 0.4. The stress intensity factor $K_{IC}$ for Victrex PEEK 450G, a similar grade of the polymer use for interleaving, is reported in literature to lie between 3 to 6 MPa·m$^{1/2}$ [24]. An average value of 4.5 MPa·m$^{1/2}$ will be used for the following analysis. Using Equation (2) and Equation (3) a plastic radius of 0.225 mm and an energy release rate of 4.8 kJ/m$^2$ can be calculated for this polymer. The result shows that the pure polymer has almost two times higher toughness than the interlaminar fracture toughness measured in the experiments in this study. Nevertheless, the theoretical matrix rich bond line thickness required to develop the fracture toughness (0.45 mm) was not tested in the experiments reported in this work, where a maximum matrix rich bond line thickness of 0.2 mm was tested. Thus, the fracture toughness is expected to keep increasing by increasing matrix rich bond line thickness.

Similar observations were made for thermoset composites [18]. For these material systems, smaller interleave thicknesses are required to achieve the maximum (i.e. polymer) toughness, which is caused by the more brittle nature of thermosets compared to thermoplastics.

The matrix rich bond line thickness after processing was observed to be not uniform, this is particularly true for the autoclaved samples where material flow occurs during processing. This non uniformity and the difficulty to distinguish between the matrix rich and matrix poor region makes it difficult to evaluate the actual matrix rich bond line thickness after processing. Besides, this non uniformity may, moreover, also be one of the causes for the unstable crack propagation observed as it most probably resulted in a non-uniform interlaminar fracture toughness along the crack path. It is known that the unstable crack propagation may occur when the crack propagates from a region of higher toughness to a region of lower toughness, as the elastic energy stored in the specimen is more than required for making the crack to propagate in a stable manner. Or more precisely formulated unstable crack propagation may occur at the locations where $dG/da$ exceeds $dR/da$ [25].

The high cooling rates observed during stamp forming may have induced a different level of crystallinity compared to the other two (slower) processing techniques, possibly affecting the measured toughness values. DSC experiments showed, however, that a non-interleaved press consolidated specimens and non-interleaved stamp formed specimens have the same level of crystallinity of approximately 35% using an enthalpy of crystallisation value of 130 (J/g) [26] with a matrix weight fraction of 34%. Although the difference in thermal history may have resulted in different crystal morphologies, this seemed to have no effect on the measured toughness.

In conclusion, it seems that the interlaminar fracture toughness is independent of the three processes used in this work. It solely depends on the interleave thickness and is not affected by fibre migration. The amount of fibres, in the fibre migration region, is too small to

constrain the plastic zone, nor does it result in excessive fibre bridging.

## 5. Conclusions

The effect of a matrix rich interface and fibre migration on the fracture toughness of fusion bonded samples was studied. For this purpose, samples were prepared using manufacturing technologies having different characteristic processing times, namely: autoclave consolidation, press consolidation, and stamp forming. Autoclave and press consolidation were considered as slow processes, while stamp forming was considered as a fast process with conditions similar to those in many welding techniques. Matrix rich bond lines with different thicknesses were obtained by interleaving matrix films at the interface between two adherents prior to fusion bonding.

Microscopy showed that two regions can be identified in the interleaved samples, namely the matrix poor adherent(s) and a matrix rich bond line. The processing time, moreover, affected the matrix rich bond line morphology. On the one hand, fibre migration from the adherents into the matrix rich bond lines was observed during (the slower) press and autoclave consolidation, resulting in a matrix rich zone with many loose fibres. On the other hand, fibre migration was prevented during (the faster) press forming, resulting in a bond line with very few or no fibres. Double cantilever beam experiments were performed and showed that the increase in the matrix rich bond line improves the fracture toughness. This increase is attributed to the development of microscale matrix plastic deformation. Moreover, it was shown that fibre migration has a negligible effect on the interlaminar fracture toughness, i.e. the toughness only depends on the matrix interleave thickness.

## 6. Acknowledgements

The authors gratefully acknowledge the financial as well as technical support from the industrial and academic members of the ThermoPlastic composites Research Center (TPRC)

529 as well as the support funding from the Province of Overijssel for improving the regional
530 knowledge position within the Technology Base Twente initiative.

## 531 7. Reference

532

[1] A. Benater and T. G. Gutowski, “Methods for fusion bonding thermoplastic composites,” *SAMPE. Quarterly,* vol. 18(1), pp. 35-42, 1986.

[2] A. P. da Costa and et al., “A review of welding technologies or thermoplastic composites in aerospace applications,” *Journal of Aerospace Technology and Management,* vol. 4.3, pp. 255-266, 2012.

[3] P. Davies and et al., “Joining and repair of a carbon fibre-reinforced thermoplastic.,” *Composites,* vol. 22.6, pp. 425-431, 1991.

[4] S. M. Todd, “Joining Thermoplastic Composite.,” *Proceedings of the 22nd International SAMPE Technical Conference,* vol. 22, pp. 383-392, 1990.

[5] A. Yousefpour, M. Hojjati and J. Immarigeon, “Fusion bonding/welding of thermoplastic composites,” *Journal of Thermoplastic Composite Materials,* vol. 17(4), pp. 303-341, 2004.

[6] M. M. Schwartz, “Joining of composite-matrix materials,” *Materials Park - ASM International,* 1994.

[7] I. Da Baere, K. Allaer, S. Jacques, W. Van Paepegem and J. Degrieck, “Interlaminar behavior of infrared welded joints of carbon fabric–reinforced polyphenylene sulfide.,” *Polymer Composites,* vol. 33, pp. 1105-1113, 2012.

[8] W. J. Cantwell and et al., “Thermal joining of carbon fibre reinforced PEEK laminates.,” *Composite Structures,* vol. 16.4, pp. 305-321, 1990.

[9] J. C. Fish and et al., “Interlaminar fracture characteristics of bonding concepts for thermoplastic primary structures.,” *AIAA journal,* vol. 30.6, pp. 1602-1608, 1992.

[10] C. Ageorges, L. Ye and M. Hou, “Advances in fusion bonding techniques for joining thermoplastic matrix composites: A review.,” *Composites - Part A: Applied Science and Manufacturing,,* vol. 32(6), pp. 839-857, 2001.

[11] R. Fracasso, M. Rink, A. Pavan and R. Frassine, “Effects of strain-rate and temperature on the interlaminar fracture toughness of interleaved PEEK/CF composites.,” *Composites Science and Technology,* vol. 61(1), pp. 57-63, 2001.

[12] O. Ishai, H. Rosenthal, N. Sela and E. Drukker, “Effect of selective adhesive interleaving on interlaminar fracture toughness of graphite/epoxy composite laminates,” *Composites,* vol. 19(1), pp. 49-54, 1988.

[13] M. Hojo, T. Ando, M. Tanaka, T. Adachi, S. Ochiai and Y. Endo, “Modes I and II interlaminar fracture toughness and fatigue delamination of CF/epoxy laminates with self-same epoxy interleaf.,” *International Journal of Fatigue,* 2006.

[14] K. Shivakumar and R. Panduraga, “Interleaved polymer matrix composites - A review.,” *54th AIAA/ASME/ASCE/AHS/ASC Structures, Structural Dynamics, and Materials Conference,* 2013.

[15] S. F. Chen and B. Z. Jang, “Fracture behaviour of interleaved fiber-resin composites." 41.1 (1991): 77-97,” *Composites Science and Technology,* vol. 41.1, pp. 77-97, 1991.

[16] A. J. Kinloch and S. J. Shaw, “The fracture resistance of a toughened epoxy adhesive,” *The Journal of Adhesion,* vol. 12(1), pp. 59-77, 1981.

[17] M. D. Banea, L. F. Da Silva and R. D. Campilho, “The effect of adhesive thickness on the mechanical behavior of a structural polyurethane adhesive.,” *The Journal of Adhesion,* vol. 91.5, pp. 331-346, 2015.

[18] S. Singh and I. K. Patridge, “Mixed-mode fracture in an interleaved carbon-fibre/epoxy composite.,” *Compos Sci Technol,* vol. 55, pp. 319-327, 1995.

[19] F. Ozdil and L. A. Carlsson, “Plastic zone estimates in mode I interlaminar fracture of interleaved composites.,” *Engineering Fracture Mechanics,* vol. 41(5), pp. 645-658, 1992.

[20] W. S. Jojnso and P. D. Mangalgiri, “Investigation of fiber bridging in double cantilever beam specimens,” *Journal of Composites Technology and Research,* vol. 9(1), p. 10, 1987.

[21] G. B. Murri, “Effect of data reduction and fiber-bridging on Mode I delamination characterization of

unidirectional composites," *Journal of Composite Materials,* vol. 48.19, pp. 2413-2424, 2014.

[22] "ISO 15114- Fibre-reinforced plastic composites - Determination of the mode II fracture resistance for unidirectionally reinforced materials using the calibrated end-loaded split (C-ELS) test and an effective crack length approach," 2014.

[23] D. Purslow, "Matrix fractography of fibre-reinforced thermoplastics, Part 1. Peel failures," *Composites*, pp. 365-374, 1987.

[24] R. Gensler, p. Béguelin, C. J. Plummer, H. Kausch and H. Münstedt, "Tensile behaviour and fracture toughness of poly(ether ether ketone)/poly(ether imide) blends.," *Polymer Bulletin,* vol. 37(1), pp. 111-118, 1996.

[25] T. W. Aifantis and E. C. Webb, "Crack growth resistance curves and stick-slip fracture inestabilities," *Mechanics Research Communications,* vol. 24, pp. 123-130, 1997.

[26] A. A. Mehmet-Alkan and J. N. Hay, "The crystallinity of PEEK composites," *Polymer,* vol. 34(16), pp. 3529-3531, 1993.

533